

Adaptive Parameter-Free Robust Learning using Latent Bernoulli Variables

Aleksandr Karakulev^{1,§} Dave Zachariah^{2,*} Prashant Singh^{1,3,*}

¹Division of Scientific Computing ²Division of Systems and Control ³Science for Life Laboratory
Department of Information Technology, Uppsala University

Abstract

We present an efficient parameter-free approach for statistical learning from corrupted training sets. We identify corrupted and non-corrupted samples using latent Bernoulli variables, and therefore formulate the robust learning problem as maximization of the likelihood where latent variables are marginalized out. The resulting optimization problem is solved via variational inference using an efficient Expectation-Maximization based method. The proposed approach improves over the state-of-the-art by automatically inferring the corruption level and identifying outliers, while adding minimal computational overhead. We demonstrate our robust learning method on a wide variety of machine learning tasks including online learning and deep learning where it exhibits ability to adapt to different levels of noise and attain high prediction accuracy.

1. Introduction

Several statistical learning problems are formulated as estimation of parameters $\theta \in \Theta$ of a probabilistic model by maximizing its likelihood function $p(\mathbf{z}|\theta)$ for observation $\mathbf{z} \sim p(\mathbf{z})$. It is more convenient to define the loss function as the negative log-likelihood $\ell_\theta(\mathbf{z}) = -\ln p(\mathbf{z}|\theta)$, and solve the equivalent minimization problem. Hence, given a training set of n independent observations $Z = \{\mathbf{z}_i\}_{i=1}^n$, the learning problem consists of finding the solution,

$$\theta_{\text{ML}} = \arg \max_{\theta \in \Theta} \prod_{i=1}^n p(\mathbf{z}_i|\theta) = \arg \min_{\theta \in \Theta} \sum_{i=1}^n \ell_\theta(\mathbf{z}_i). \quad (1)$$

However, real-world data is often corrupted – samples arise from a mixture of the true distribution $p(\mathbf{z})$ and a corrupting source $q(\mathbf{z})$,

$$\tilde{p}(\mathbf{z}) = (1 - \varepsilon)p(\mathbf{z}) + \varepsilon q(\mathbf{z}), \quad (2)$$

leading to a suboptimal solution θ_{ML} . In this contaminated mixture, outliers $\mathbf{z} \sim q(\mathbf{z})$ may result from inaccurate measurements, errors or oversight in data acquisition or labeling, or even malicious attacks. The situation is further complicated by the fact that the corrupting distribution $q(\mathbf{z})$ is typically unknown, and the level of corruption ε , difficult to determine. Equation (2) used herein follows the well-known Huber contamination model from the robust statistics literature [10, 15]. Existing approaches require an estimation of the noise structure or the corruption level ε . This imposes restrictions on using these methods in settings where such pre-processing becomes impractical, e.g., in online learning, wherein the assumption about ε needs to be optimized in continuously arriving data. In Figure 1, we show an example: the accuracy of binary classification trained on data that is continuously collected from the HAR dataset [8], and subsequently corrupted with varying number of randomly flipped labels in each batch (details in Section 4.2).

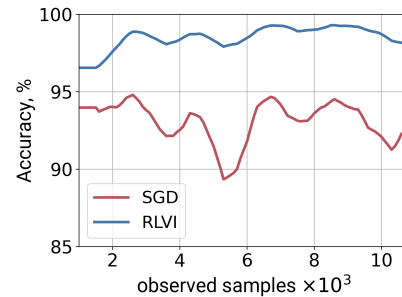


Figure 1. Classification of online streaming data with varying number of outliers. The parameter-free nature of our approach (RLVI) allows for automatic identification of outliers when learning from batches of data with different ε . Our method is robust and thus has higher accuracy than the standard stochastic optimization of the likelihood (SGD).

Contribution. We present a principled parameter-free robust learning approach for settings involving likelihood maximization that introduces minimal computational overhead, and is general in applicability with respect to model or

[§]aleksandr.karakulev@it.uu.se

*Co-senior authors

problem type. We demonstrate the approach in online learning and deep learning settings, where it meets or exceeds state-of-the-art results on benchmark datasets.

Related work. While some approaches address learning from corrupted data with a special loss function, e.g., the Huber loss [9], others construct certain criteria to separate samples from the true distribution, from the corrupted ones [1, 2]. Recently, new general approaches, such as SEVER [5] and Robust Risk Minimization (RRM) [18], were introduced. SEVER is a general gradient-based learning method that penalizes the gradient components of the loss function corresponding to outliers. RRM involves obtaining sample weights from the constraint on the entropy of a re-weighted empirical distribution, and minimizing the corresponding modified empirical risk. Both methods are not model-specific and do not require the exact value of ε , rather only an upper-bound. Robust Risk Minimization does not require calibrating multiple hyperparameters like SEVER, but requires assessing the level of corruption by estimating its maximum value.

In the recent past, learning from corrupted data has also received attention in the field of deep learning, and several approaches have been proposed to train a neural network in a robust way. For instance, one can use the correction of the regular loss function [19, 24]. Alternatively, some approaches directly estimate the noise transition matrix [6, 19]. Others utilize an additional neural network to identify and prevent overfitting of the initial model, as in [11], and to obtain a better accuracy by exchanging the information between two simultaneously trained networks, as in [7] and [20]. Another option is to combine techniques that are specific to deep learning – early-stopping [22] or dropout [23], with a criterion that aims to eliminate corrupted samples. However, training a neural network in the regular context where the contamination issue is not addressed, already requires certain hyperparameters to improve generalization, e.g., learning rate, batch-size, number of layers, etc. The aforementioned approaches introduce additional parameters to combat the problem of corrupted labels, including ε , which makes their performance dependent on the efficacy of these parameters and the underlying assumptions.

Robust Learning via Variational Inference. The proposed approach, denoted as RLVI, employs latent Bernoulli variables to identify corrupted and non-corrupted training data samples. Distribution of the latent variables is characterized from training data by maximizing the variational lower bound of marginal likelihood (variational inference) [16]. This allows detection of outliers and computation of the optimal corruption level ε automatically, subsequently learning the model θ in a robust way. The problem formulation entailing RLVI is theoretically simple, and also leads to efficient and straightforward implementation.

The paper is structured as follows. Section 2 presents the

problem formulation – introducing the latent variables enabling the marginal likelihood approach. Section 3 describes the Expectation-Maximization based method, realizing variational inference, and its extension to stochastic optimization for online learning and deep learning problems. Section 4 validates the efficacy of the proposed approach against existing approaches on standard statistical learning problems (linear regression and classification, PCA, online learning) [5, 10, 18] and image classification [7, 20, 22, 23].

2. Problem Formulation

Central to our approach is the introduction of a latent variable t_i for each observation $z_i \in Z$ such that,

$$t_i = \begin{cases} 1, & z_i \sim p(z), \\ 0, & z_i \sim q(z). \end{cases} \quad (3)$$

Knowing the values of these variables would allow us to avoid minimizing the losses on outliers in the dataset in (1) by simply dropping the corresponding terms from the sum. In other words, latent variables enable us to define a likelihood function with respect to the non-corrupted data, such that,

$$p(Z|\mathbf{t}, \theta) = \prod_{i=1}^n p(z_i|\theta)^{t_i}, \quad (4)$$

where $\mathbf{t} = [t_1, t_2, \dots, t_n]$. Optimization with respect to this likelihood function implies a combinatorial search over the latent variables \mathbf{t} , which is computationally infeasible even for moderate n .

We observe, however, that the contamination model (2) implies that each sample has a probability ε of being corrupted. Thus we have the following distribution over \mathbf{t} ,

$$p(\mathbf{t}|\varepsilon) = \prod_{i=1}^n (1 - \varepsilon)^{t_i} \varepsilon^{1-t_i}. \quad (5)$$

This prior information enables us to marginalize out the latent variables and obtain the *marginalized* likelihood,

$$p(Z|\theta, \varepsilon) = \sum_{\mathbf{t}} p(Z|\mathbf{t}, \theta)p(\mathbf{t}|\varepsilon). \quad (6)$$

Then the maximum marginal likelihood solution,

$$\theta_\star = \arg \max_{\theta} \max_{\varepsilon} p(Z|\theta, \varepsilon), \quad (7)$$

addresses the problem of robust learning of θ while obviating the need for specifying ε or a combinatorial search over \mathbf{t} . We now turn to developing a method to solve (7) in an efficient manner.

3. Method

We begin by introducing a variational lower bound on the marginal likelihood in (7) and then turn to implementation-specific aspects of the derived method.

Variational inference. To solve the formulated optimization problem, we need a tractable way to compute the sum over t in (6). Using Bayes' rule, we express the marginal likelihood as,

$$p(Z|\theta, \varepsilon) = \frac{p(Z|t, \theta)p(t|\varepsilon)}{p(t|Z, \theta, \varepsilon)}, \quad (8)$$

where the denominator is the posterior distribution of latent variables t given the data Z , specified model θ , and the corruption level ε . As this posterior is intractable, we consider its variational approximation denoted $r(t|\pi)$. Specifically, we use a distribution of n independent Bernoulli variables with probabilities $\pi = [\pi_1, \dots, \pi_n]$,

$$r(t|\pi) = \prod_{i=1}^n \pi_i^{t_i} (1 - \pi_i)^{1-t_i}. \quad (9)$$

Consequently, instead of maximizing the marginal likelihood function $p(Z|\theta, \varepsilon)$ directly, we apply the variational inference framework, and optimize the so-called evidence lower-bound (ELBO) [16]. This lower bound has the following general form,

$$\ln p(Z|\theta, \varepsilon) \geq \mathbb{E}_{r(t|\pi)} \left[\ln p(Z|\theta, t) \right] - \text{KL} \left[r(t|\pi) \parallel p(t|\varepsilon) \right], \quad (10)$$

where the first term is the expected value of the log-likelihood over latent variables and the second term is the Kullback–Leibler divergence between the variational approximation and the prior. The first ELBO term can be rewritten using the loss function $\ell_\theta(z_i) = -\ln p(z_i|\theta)$,

$$\mathbb{E}_{r(t|\pi)} \left[-\sum_{i=1}^n t_i \ell_\theta(z_i) \right] = -\sum_{i=1}^n \pi_i \ell_\theta(z_i), \quad (11)$$

where the equality follows from (9). This term corresponds to an average loss with non-uniform sample weights, with π_i representing the probability of sample i being non-corrupted.

The second ELBO term consists of the closed form,

$$\text{KL} \left[r \parallel p \right] = \sum_{i=1}^n \pi_i \ln \frac{\pi_i}{1 - \varepsilon} + (1 - \pi_i) \ln \frac{1 - \pi_i}{\varepsilon}. \quad (12)$$

Note that corruption level does not appear in the first term of the ELBO, and we can optimize the KL-divergence w.r.t. ε directly and independently of the model θ . This results in $n(1 - \varepsilon) = \sum_i \pi_i$. In other words, parameters π_i defining the probability of each sample being non-corrupted, should sum up to the number of non-corrupted samples. We can therefore express the optimal corruption fraction as,

$$\varepsilon = 1 - \langle \pi \rangle, \quad (13)$$

where $\langle \pi \rangle$ is the average of the Bernoulli probabilities. Hence, we arrive at the following objective – the negative ELBO expressed as,

$$\mathcal{L}(\theta, \pi) = \sum_{i=1}^n \pi_i \ell_\theta(z_i) + \pi_i \ln \frac{\pi_i}{\langle \pi \rangle} + (1 - \pi_i) \ln \frac{1 - \pi_i}{1 - \langle \pi \rangle}. \quad (14)$$

In conclusion, the objective in (7) is replaced by the optimum of its variational bound, i.e.,

$$\theta_{\text{VI}} = \arg \min_{\theta \in \Theta} \min_{\pi \in [0;1]^n} \mathcal{L}(\theta, \pi). \quad (15)$$

Numerical optimization. The resulting optimization problem is solved using the block-wise Algorithm 1, which follows the general Expectation-Maximization (EM) scheme [3]. The E-step consists of minimizing $\mathcal{L}(\theta, \pi)$ in π for fixed parameters θ . In the M-step, the inferred probabilities are used to maximize the re-scaled log-likelihood, $-\sum_{i=1}^n \pi_i \ell_\theta(z_i)$. As an example, in case of linear regression the latter step solves a weighted least-squares problem. For a classification task, we minimize the cross-entropy loss corrected with sample weights.

Note that the E-step can be performed efficiently, as the objective $\mathcal{L}(\theta, \pi)$ is convex in π (proof is in the Appendix). Therefore, to find the optimal parameters π for a fixed model, the derivative of $\mathcal{L}(\theta, \pi)$ is equated to zero w.r.t. π_j for all $j = 1, \dots, n$,

$$\frac{\partial \mathcal{L}}{\partial \pi_j} = 0 \iff \pi_j = \left(1 + \frac{1 - \langle \pi \rangle}{\langle \pi \rangle} e^{\ell_\theta(z_j)} \right)^{-1}. \quad (16)$$

This is a system of nonlinear equations for π , which we solve with the fixed-point iteration procedure,

$$\pi_j^{\text{new}} = \left(1 + \frac{1 - \langle \pi^{\text{old}} \rangle}{\langle \pi^{\text{old}} \rangle} e^{\ell_\theta(z_j)} \right)^{-1}. \quad (17)$$

Here, for the mean weight, we use the value from the previous fixed-point iteration and compute π_j^{new} independently with simple vector operations that scale well for large data.

Algorithm 1 RLVI: robust learning from corrupted data

- 1: **Input:** data $Z = \{z_i\}_{i=1}^n$
 - 2: $\theta^0 \leftarrow \arg \min_{\theta \in \Theta} \sum_{i=1}^n \ell_\theta(z_i)$ $\triangleright \pi^0 = 1$
 - 3: **for** $k = 1, 2, \dots$ **do**
 - 4: Evaluate $\ell_\theta(z_i)$ for each $z_i \in Z$ using θ^{k-1}
 - 5: $\pi^k \leftarrow$ fixed-point iterations (17) \triangleright E-step
 - 6: $\theta^k \leftarrow \arg \min_{\theta \in \Theta} \sum_{i=1}^n \pi_i^k \ell_\theta(z_i)$ \triangleright M-step
 - 7: **if** $\|\theta^k - \theta^{k-1}\| \leq \textit{tolerance}$ **then**
 - 8: **return** θ^k
-

Stochastic approximation. The formulated objective $\mathcal{L}(\theta, \pi)$ alleviates the need to know or assess ε , which is particularly useful when ε is not fixed, such as in the online learning setting. Another useful property of this variational bound is its structure – with respect to θ , the function consists of n independent terms, just as the standard likelihood function, which can be employed by stochastic optimization of $\mathcal{L}(\theta, \pi)$. That is, if one does not have access to the full dataset but only to its batches, the M-step in Algorithm 1 can be replaced with a stochastic gradient descent (SGD) update,

$$\theta^k = \theta^{k-1} - \alpha \sum_{i=1}^b \pi_i^k \nabla \ell_\theta(z_i), \quad (18)$$

where the loss function and, therefore, the gradient components for each batch of b samples $\{z_i\}_{i=1}^b$ are re-weighted with $\pi^k \in [0; 1]^b$. The latter are computed using the corresponding loss values $\ell_\theta(z_i)$, $z_i = 1, \dots, b$, at the preceding E-step with (17). Batch minimization of $\mathcal{L}(\theta, \pi)$, in effect, corresponds to a stochastic variant of the EM algorithm (see stepwise EM in [16]).

Truncation as a form of regularization. Since the objective in RLVI is suitable for stochastic optimization, our robust learning approach can also be used in deep learning, where SGD-like approaches are dominant. However, neural networks are overparameterized models and thus are prone to overfitting, which in theory (and in practice – see Figure 5) hinders the performance of RLVI. Indeed, if we substitute $\ell_\theta(z_i) \approx 0$ for all samples into the stationary point condition (16), we find the corresponding minimum for π ,

$$\pi_i^* = \left(1 + \frac{\varepsilon}{1 - \varepsilon} e^{\ell_\theta(z_i)}\right)^{-1} = 1 - \varepsilon, \quad i = 1, \dots, n. \quad (19)$$

That is, as soon as overfitting commences, the marginal likelihood approach treats corrupted samples as non-corrupted since overparameterized models are able to attain a high likelihood for outliers as well. Nevertheless, as is generally the case, to prevent overfitting, one can use regularization of the loss function. In this work, we introduce regularization to the RLVI algorithm based on the obtained posterior approximation, making the algorithm effective in the overparameterized regime as well. Namely, samples that have a low probability of being non-corrupt, $\pi_i < \tau$, are eliminated from SGD updates. This hard truncating approach raises two questions – when to apply it and how to select the decision boundary τ . Both questions are formally resolved with no additional parameters required, as described in Section 4.3.

4. Experiments

The proposed RLVI method is compared to existing approaches in three problem settings: standard parameter estimation, online learning, and deep learning.

4.1. Benchmark on standard learning problems

Problem	dimension	n	ε	$\tilde{\varepsilon}$
LinReg	$x \in \mathbb{R}^{10}, y \in \mathbb{R}, \theta \in \mathbb{R}^{10}$	40	0.2	0.4
LogReg	$x \in \mathbb{R}^2, y \in \{0, 1\}, \theta \in \mathbb{R}^3$	100	0.05	0.3
PCA	$z \in \mathbb{R}^2, \theta \in \{\mathbb{R}^2 : \ \theta\ = 1\}$	40	0.2	0.4
Cov	$z \in \mathbb{R}^2, \theta = (\mu, \Sigma)$	50	0.2	0.3

Table 1. Settings for experiments, reproduced from [18] – θ is a parametric model; x , y , and z denote synthetic data (n samples) contaminated with $\varepsilon \cdot n$ outliers, and $\tilde{\varepsilon} \geq \varepsilon$ is the upper-bound used for HUBER, SEVER, and RRM.

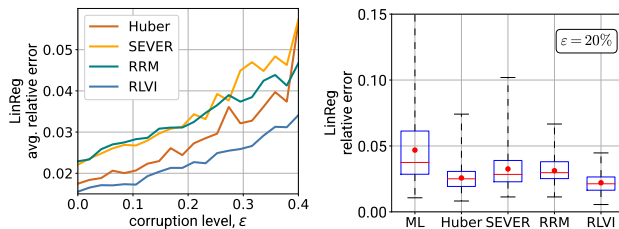


Figure 2. Linear regression. *Left.* Average relative error versus varying ε . *Right.* Box plot of relative error for $\varepsilon = 20\%$. Each box spans the 25th to 75th quantiles; red dots depict the means. For both plots, 100 Monte Carlo runs are used. RLVI obtains higher average accuracy and tighter confidence intervals.

First, we demonstrate that our method is applicable to different maximum likelihood problems and achieves higher model accuracy over contemporary alternatives. Thereto, we reproduce the experiments from [18] comparing various algorithms for robust learning on four problems: linear regression, logistic regression, dimensionality reduction using principal component analysis (PCA), and covariance estimation. Since each problem can be formulated as likelihood maximization, we define the corresponding loss functions as the negative log-likelihood. In the experiments, synthetic data (n samples) is generated from the mixture of $p(z)$ and $q(z)$ with a fixed ratio of outliers ε using the specified model θ^* . The optimal model $\hat{\theta}$ is estimated using different algorithms: standard ML, HUBER (method tailored for linear regression) [25], SEVER [5], RRM [18], and RLVI. The general settings for each problem are summarized in Table 1; the reader is referred to [18] for more details, including specifics of distributions used as true and corrupted. Subsequently, we perform 100 Monte Carlo runs and plot the statistics for corresponding errors with boxplots. For linear regression, the results also include average relative error for ε varying in $[0; 0.4]$ – again, 100 Monte Carlo runs were used for each fixed ε . Results are shown in Figures 2 and 3.

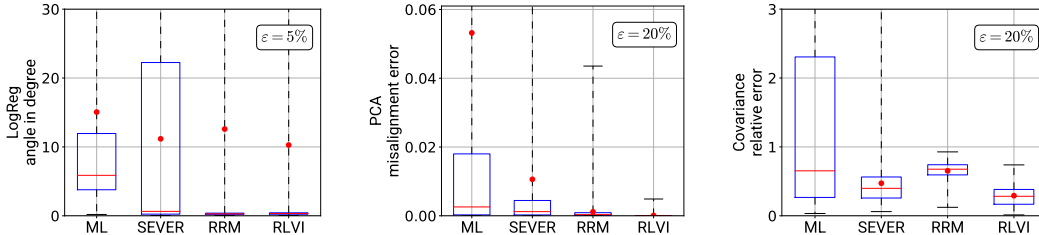


Figure 3. *Left*. Logistic regression: box plot of angle in degrees between the true separating hyperplane θ^* and estimates $\hat{\theta}$. *Middle*. PCA: box plot of misalignment errors $1 - |\cos(\hat{\theta}^\top \theta^*)|$ for the subspace spanned by the first principal component. *Right*. Covariance estimation: box plot of relative errors $\|\hat{\theta} - \theta^*\|_F / \|\theta^*\|_F$, where $\theta^* = (\mu, \Sigma)$ is the true mean and covariance, and $\hat{\theta}$ is the corresponding estimate.

RLVI achieves better average accuracy and tighter confidence intervals than competing methods. Figure 2 depicts the results of linear regression for different corruption levels. It can be seen that RLVI performs slightly but consistently better than other approaches, including the case of no corruption $\varepsilon = 0$, owing to the ability of RLVI to automatically adjust to an arbitrary number of corrupted samples.

4.2. Online learning

To further evaluate RLVI’s adaptivity, we apply it to online learning – the setting where ε changes dynamically. Online learning is used when dealing with, for example, signals from remote sensors, user clicks on a website, daily weather conditions, etc. In such cases, data is being collected sequentially and the model is incrementally learned from each new set of observations. This allows continuous refinement of the model and out-of-core inference when the dataset is too large to be stored and handled entirely.

As described in Section 3, the objective $\mathcal{L}(\theta, \pi)$ in RLVI allows for an incremental learning scheme by replacing the M-step of EM algorithm with an update of stochastic gradient descent: $\theta^k = \theta^{k-1} - \alpha \sum_{i=1}^b \pi_i^k \nabla \ell_\theta(z_i)$. Here, parameters π^k are computed at the E-step with (17). The computational overhead over the standard stochastic likelihood maximization is not significant: the fixed-point algorithm only involves $O(b)$ vectorized operations at each SGD step.

We consider the Human Activity Recognition dataset from [8] containing 24,075 measurements from smartphone sensors. Each measurement $z_i = (x_i, y_i)$ consists of $x_i \in \mathbb{R}^{60}$ features extracted from accelerometers during different human activities: Sitting, Standing, Walking, Running, and Dancing. We perform binary classification and towards that end, partition the five initial labels into two: resting state ($y = 0$) and active state ($y = 1$). To simulate a data stream, at each iteration we retrieve data in batches of size $2b$, where $b = 100$ samples are used for training and another $b = 100$ samples serve performance evaluation. To introduce noise, we corrupt the data in each training batch by randomly flipping ε percent of positive labels. Moreover, the corruption level ε changes in each iteration. Since we are

testing the robustness of RLVI against corruption, we focus specifically on variation of noise – not on the gradual change of θ (concept drift) or other possible challenges related more to the method to learn θ incrementally. For each batch, ε is sampled from a linearly transformed Beta distribution (called PERT [12]) that is simple to parameterize with three values, so that the samples are within the interval $[\varepsilon_{\min}, \varepsilon_{\max}]$ with the mode $\varepsilon_{\text{mode}}$. To simulate a typical case, we set $\varepsilon_{\min} = 0$, $\varepsilon_{\max} = 0.3$, and $\varepsilon_{\text{mode}} = 0.1$. Thus, the ratio of corrupted labels in each batch varies according to the distribution in Figure 4.

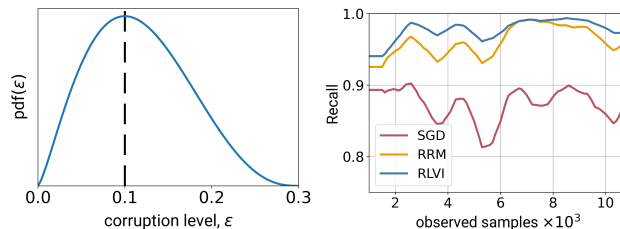


Figure 4. Online classification. *Left*. Distribution of corruption level across batches of streaming data. *Right*. Recall (true positive rate) on left-out data versus total number of observed samples – the metric is smoothed with a moving average filter.

Since RRM is also based on block-wise optimization, it can similarly be implemented as incremental learning, where inference for θ consists of anti-gradient steps minimizing the modified empirical risk for each batch. Hence, the experiments compare three versions of online classification: the standard stochastic maximization of the likelihood (SGD), incremental minimization of the risk function defined in RRM [18] with a threshold for ε set to $\varepsilon_{\max} = 0.3$, and the presented variational inference approach (RLVI).

Classification performance is evaluated with recall (true positive rate) computed for 100 test samples in each iteration. Figure 4 shows the evolution of recall smoothed with a moving average filter with a window of 10 batches (also, see the smoothed accuracy curve in Figure 1). It can be seen that standard SGD clearly suffers from label corruption,

with RRM being affected to a lesser extent. RLVI attains consistently higher accuracy and recall values as it does not depend on a global estimate of the noise magnitude, and robustly evaluates it from incoming data.

4.3. Overparameterized model

We now extend RLVI to learning an overparameterized model and, as an example, consider image classification using a convolutional neural network and corrupted training labels.

Existing approaches. State-of-the-art performance is achieved in this setting by methods that identify and distill corrupted samples based on some criterion. The algorithm Co-teaching [7], for example, is based on training two neural networks in parallel and learning only on the samples that attain a small loss for both models. The JoCoR approach [20] also trains two models but aims to reduce the diversity between their predictions. Due to simultaneous training of two models, Co-teaching and JoCoR effectively double the computational time. CDR [22] in contrast, trains one model – it employs weight decay to diminish the impact of network parameters that overfit to corrupted samples, and early-stopping using a validation set. The recent algorithm USDNL [23] estimates prediction uncertainty for training samples using dropout in a single network, thus identifying the samples with corrupted labels. Each of the above methods combines its own criterion for outliers with a schedule to gradually consider fewer samples and thus account for model overfitting occurring in later epochs. This schedule is a non-decreasing function defined with the corruption level ε (assumed to be known in advance) so that, by the end of training, only $(1 - \varepsilon)$ ratio of the training set is being used.

Regularization. As described in Section 3, to prevent overfitting, we implement regularization using hard truncation: $\pi_i < \tau \implies \pi_i = 0$. Consequently, we need to evaluate when to apply this regularization, and how to select the truncation boundary τ . The answer to the first question is straightforward: regularization is to be applied when the model begins to overfit, which in practice can be identified with a drop in prediction accuracy on a noisy validation set. As studied empirically [11, 17, 22], neural networks first fit the true distribution. In other words, before the network reaches an overfitting stage, the loss on corrupted samples is not reduced, and computed quantities π_i allow for differentiation of outliers as described in the first sections.

To answer the second question, we note that in light of corrupted samples, regularization of an overparameterized model gives rise to asymmetrical errors. On one hand, if a fraction of non-corrupted samples is identified as corrupted and thus is excluded from optimization with the decision rule $\pi_i < \tau \implies \pi_i = 0$, the loss is minimized on a smaller subset of ‘clean’ samples. Consequently, the model does not fit the training set perfectly. In contrast, if corrupted samples

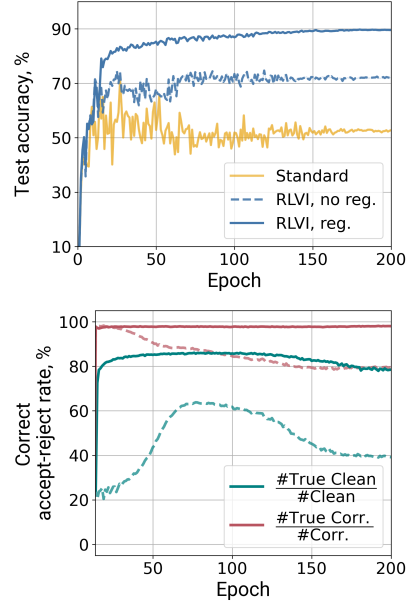


Figure 5. Image classification on CIFAR10 corrupted with synthetic noise (pairflip with $\varepsilon = 45\%$). *Top*. Accuracy on the clean testing set for standard SGD and RLVI. *Bottom*. Percentage of corrupted and non-corrupted samples correctly identified with the decision rule ($\pi_i < \tau$). In both plots, the dashed line corresponds to RLVI with no regularization – solid line indicates that truncation ($\pi_i < \tau \implies \pi_i = 0$) is used to set the corresponding terms in anti-gradient updates to zero. Decision boundary τ is computed from the bounded type II error criterion (20). Regularization based on reducing type II error minimizes overfitting, making differentiation of corrupted and non-corrupted data points more effective, ultimately improving test accuracy.

are treated as ‘clean’, the model adapts to the contamination term $q(z)$ thereby learning the wrong pattern. To account for a higher cost of the latter, type II error, the optimal threshold τ^* is obtained from the condition that the error is fixed at the admissible level of 5% (typically a standard choice in statistical test theory). Furthermore, the type II error is approximated using the obtained posterior $r(t|\pi)$ from the variational inference formulation,

$$\frac{\mathbb{E}_r[\#\text{False Clean}]}{\mathbb{E}_r[\#\text{Corrupted}]} = \frac{\sum_{i=1}^n (1 - \pi_i) \mathbb{1}[\pi_i \geq \tau]}{\sum_{i=1}^n (1 - \pi_i)} \leq 0.05. \quad (20)$$

Here, the numerator equals the expected number of corrupted samples considered as ‘clean’, and the denominator is the expected total number of corrupted samples, with respect to posterior probabilities π . To increase the number of samples to be used for learning, one can select the largest $\tau \in \{\pi_1, \pi_2, \dots, \pi_n\}$ satisfying the inequality above.

Such a solution can be readily found after sorting the array $\pi \in [0; 1]^n$ in $O(n \ln n)$ time. Figure 5 presents an example of image classification on CIFAR10 with randomly flipped labels (read about ‘pairflip’ synthetic noise below). It illustrates how the introduced regularization functions in practice: if no regularization is used, the proportion of identified noisy observations decreases as the model gradually fits $q(\mathbf{z})$, thus attaining lower test accuracy. But with regularization, differentiation of corrupted and non-corrupted data points according to π_i remains effective during all iterations, which leads to better generalization. In the Appendix, we provide similar plots for other types and levels of noise.

Resulting algorithm. We now introduce Algorithm 2 that implements RLVI as stochastic gradient optimization of neural network parameters θ . It achieves robustness by maximizing the evidence lower-bound (15) instead of regular maximization of the likelihood. The latter employs parameters π_i that represent probability of each sample to be non-corrupted. These parameters are updated at the end of each epoch using efficient fixed-point iterations (17). To prevent model’s overfitting to corrupted samples, the algorithm eliminates gradient terms corresponding to low π_i . Threshold for truncation is re-computed across epochs as a non-decreasing value from the type II error criterion (20).

Algorithm 2 RLVI: robust training of neural networks

- 1: **Input:** training set $Z_{tr} = \{\mathbf{z}_i\}_{i=1}^n$, noisy validation set Z_{val} , learning rate α , batch size b
 - 2: $\theta \leftarrow$ initialize neural network parameters
 - 3: $\pi_i \leftarrow 1, i = 1, \dots, n$
 - 4: $L \leftarrow$ empty array of size n \triangleright to store $\ell_{\theta}(\mathbf{z}_i), \mathbf{z}_i \in Z_{tr}$
 - 5: *overfit* \leftarrow False
 - 6: $\tau \leftarrow 0$
 - 7: **for** epoch = 1, 2, ..., n_{epochs} **do**
 - 8: **for** $\mathcal{I}_b \sim U\{1, \dots, n\}$ **do** \triangleright batch of b indices
 - 9: $L_i \leftarrow \ell_{\theta}(\mathbf{z}_i), i \in \mathcal{I}_b$ \triangleright store loss value
 - 10: $\theta \leftarrow \theta - \alpha \sum_{i \in \mathcal{I}_b} \pi_i \nabla \ell_{\theta}(\mathbf{z}_i)$
 - 11: $\pi \leftarrow$ fixed-point (17) using loss values in L
 - 12: **if** *overfit* **then** \triangleright regularization
 - 13: $\tau^* \leftarrow \max\{\pi_1, \dots, \pi_n\}$, s.t. error bound (20)
 - 14: $\tau \leftarrow \max(\tau, \tau^*)$ \triangleright can only increase
 - 15: $\pi_i \leftarrow \pi_i$ **if** $\pi_i \geq \tau$ **else** 0
 - 16: **else**
 - 17: *overfit* \leftarrow True **if** accuracy on Z_{val} dropped
 - 18: **Output:** θ
-

Synthetic noise. To test the algorithm, we conduct the experiments in image classification using convolutional neural

networks and cross-entropy loss as ℓ_{θ} . The datasets being used are MNIST [14], that contains hand-written digits, and CIFAR10 and CIFAR100 [13] – both containing the same images that are classified into ten and one hundred categories respectively. Subsequently, the training labels in these datasets are corrupted with three types of synthetic noise: symmetric, asymmetric, and pairflip. These noise types have been commonly used in previous works [7, 20, 22, 23]. Training was performed with the conventional values of hyperparameters for each case. Namely, for MNIST, we used the LeNet architecture and the SGD optimizer with momentum 0.9, weight decay of strength 10^{-3} , and linearly decaying learning rate (initial rate 0.01). LeNet was trained for 100 epochs with the batch size 32. For CIFAR10 and CIFAR100, the architecture used was ResNet18 and ResNet34 respectively, trained with the SGD optimizer, with momentum 0.9 and weight decay of strength $5 \cdot 10^{-4}$, that employed cosine annealing to decay a learning rate (initial rate 0.01). Optimization was performed for 200 epochs with batches of size 128. Furthermore, we compare the attained classification accuracy on the test set with the standard likelihood maximization approach and four recently proposed alternative methods: Co-teaching, JoCoR, CDR, and USDNL. For CDR and RLVI, 10% of the training data was left-out as a validation set. For RLVI, we identify overfitting, and thus start applying regularization, as soon as validation accuracy at the current epoch becomes less than the average of its two previous values. In contrast, CDR uses a validation set for early-stopping: optimization should conclude if the validation accuracy exceeds some specified threshold. To avoid any uncertainty in selecting this threshold, for CDR, we report the test accuracy that corresponds to the lowest validation loss during all epochs. For all other methods, we consider accuracy at the last epoch as a final result. For Co-teaching, JoCoR, CDR, and USDNL, we used their default hyperparameters related to robust learning, including the same schedule for the ratio of considered samples during epochs, as defined in [7], deduced from the true noise level employed. Also, since USDNL is based on uncertainty estimation using dropout, for USDNL specifically, we used variations of LeNet, ResNet18, and ResNet34 with dropout layers, where dropout rate was set to 0.25 (as in the original paper [23] – but for another architecture).

The results are presented as mean \pm standard deviation over five runs with random initialization of network’s parameters. Table 2 shows that RLVI, with the described regularization, attains results competitive with alternative approaches. Also, because the number of training samples n in deep learning is typically much smaller than the number of network’s parameters in θ , the additional steps in Algorithm 2 that involve π (fixed-point iterations and truncation) do not significantly increase the computational time compared to standard SGD. Table 3 shows the average time per epoch when training on CIFAR100.

Table 2. Test accuracy (%) of image classification after training on datasets corrupted with synthetic noise. The means and standard deviations provided are the result of five random initializations. The best mean results are in bold.

Dataset	Method	Symmetric		Asymmetric		Pairflip	
		20%	45%	20%	45%	20%	45%
MNIST	Standard	95.66±0.28	87.47±0.82	98.29±0.14	87.73±0.65	97.21±0.41	69.26±3.65
	Co-teaching	96.62±0.08	96.68±0.07	95.94±0.06	93.40±0.42	96.19±0.10	92.91±0.43
	JoCoR	99.07±0.05	98.38±0.10	99.02±0.05	95.21±3.70	98.96±0.09	91.06±5.01
	CDR	98.81±0.09	98.27±0.09	99.14±0.05	94.35±1.29	98.95±0.06	87.55±1.26
	USDNL	98.38±0.12	97.72±0.13	98.32±0.12	95.83±0.64	98.23±0.09	89.94±1.62
	RLVI	99.10±0.06	98.70±0.18	98.90±0.22	98.69±0.05	99.10±0.07	98.52±0.07
CIFAR10	Standard	83.36±0.35	60.22±0.28	87.26±0.40	75.03±0.28	81.14±0.43	52.30±0.85
	Co-teaching	87.55±0.38	83.70±0.46	86.98±0.26	64.84±0.87	86.57±0.21	67.38±2.93
	JoCoR	90.42±0.07	86.33±0.23	90.60±0.19	76.94±2.56	89.25±0.30	72.53±3.57
	CDR	85.57±0.38	77.83±0.30	87.98±0.61	75.99±1.95	87.34±0.34	68.13±2.03
	USDNL	88.65±0.21	83.33±0.23	88.36±0.33	74.62±0.70	87.05±0.24	66.49±2.45
	RLVI	92.30±0.14	88.69±0.33	91.73±0.12	76.96±0.50	92.15±0.27	89.13±0.29
CIFAR100	Standard	61.96±0.11	42.36±0.80	62.88±0.20	39.91±0.58	62.62±0.53	38.94±0.42
	Co-teaching	58.74±0.66	48.11±1.01	54.32±0.22	34.53±0.68	56.27±0.60	34.47±0.97
	JoCoR	69.43±0.25	62.37±0.94	62.93±0.60	38.68±0.83	65.90±0.35	40.94±0.70
	CDR	61.57±0.41	46.31±0.81	62.89±0.30	39.47±0.75	61.27±2.23	38.55±0.22
	USDNL	64.96±0.56	53.82±1.15	59.12±0.10	36.44±0.93	61.76±1.01	35.81±0.20
	RLVI	69.64±0.55	64.11±0.79	69.33±0.83	55.76±2.12	69.25±0.77	55.77±1.01

Table 3. Time per one epoch (in seconds) when training on corrupted CIFAR100: mean ± standard deviation over 200 epochs.

Standard	Co-teaching	JoCoR
8.82±0.08	17.91±0.35	18.11±0.11
CDR	USDNL	RLVI
13.88±0.35	9.40±0.22	10.52±0.56

Real noise. To demonstrate how RLVI performs in a naturally noisy setting, we train ResNet50 (pre-trained on ImageNet [21]) on the challenging dataset Food101 [4] consisting of 101 food categories. For each class, 250 testing images were cleaned manually, while the remaining 750 training images per class still contain outliers. We use the Adam optimizer, a multi-step learning rate schedule (starting from 10^{-3}), weight decay 10^{-4} , and batch-size 32.

In the real setting, the true ϵ is unknown and has to be optimized for Co-teaching, JoCoR, CDR, and USDNL. Figure 6 shows that by varying ϵ for alternative methods (from a large 20% – to a moderate 3% value), one can increase model performance. In contrast, RLVI improves over the standard approach without the need for additional optimization of the hyperparameter. In the Appendix, we provide results for other values of ϵ for comparison.

Our implementation of the described experiments, including existing methods used for comparison, is available at github.com/akarakulev/rlvi.

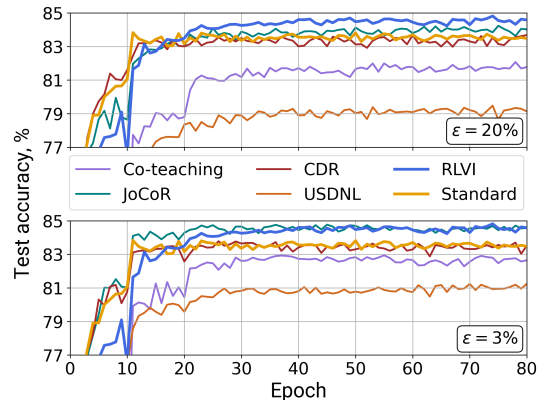


Figure 6. Test accuracy (%) for Food101, using high and low ϵ .

5. Conclusions

We presented the novel robust learning algorithm RLVI for likelihood maximization problems with corrupted datasets. It leverages variational inference to identify corrupted samples using latent Bernoulli variables. This alleviates the need for specifying hyperparameters such as the corruption level, which existing approaches rely on. RLVI can also be implemented as stochastic optimization, which makes it adaptive and applicable to learning from data with varying noise and out-of-core inference for large datasets. We demonstrated the effectiveness of the method on benchmark test problems in both – traditional statistical learning, as well as online and deep learning settings. The proposed RLVI algorithm meets or exceeds performance across considered experimental settings in a parameter-free and efficient manner.

Acknowledgements

The computations/data handling were enabled by the Berzelius resource provided by the Knut and Alice Wallenberg Foundation at the National Supercomputer Centre, and by the National Academic Infrastructure for Supercomputing in Sweden (NAISS) at Chalmers e-Commons at Chalmers, and Uppsala Multidisciplinary Center for Advanced Computational Science (UPPMAX) at Uppsala University, partially funded by the Swedish Research Council through grant agreement nos. 2022-06725 and 2018-05973. DZ acknowledges support from the Swedish Research Council through grant agreement no. 2018-05040.

References

- [1] Kush Bhatia, Prateek Jain, and Purushottam Kar. Robust regression via hard thresholding. *Advances in neural information processing systems*, 28, 2015. [2](#)
- [2] Kush Bhatia, Prateek Jain, Parameswaran Kamalaruban, and Purushottam Kar. Consistent robust regression. *Advances in Neural Information Processing Systems*, 30, 2017. [2](#)
- [3] Christopher M Bishop and Nasser M Nasrabadi. *Pattern recognition and machine learning*. Springer, 2006. [3](#)
- [4] Lukas Bossard, Matthieu Guillaumin, and Luc Van Gool. Food-101—mining discriminative components with random forests. In *Computer Vision—ECCV 2014: 13th European Conference, Zurich, Switzerland, September 6–12, 2014, Proceedings, Part VI 13*, pages 446–461. Springer, 2014. [8](#)
- [5] Ilias Diakonikolas, Gautam Kamath, Daniel Kane, Jerry Li, Jacob Steinhardt, and Alistair Stewart. Sever: A robust meta-algorithm for stochastic optimization. In *International Conference on Machine Learning*, pages 1596–1606. PMLR, 2019. [2](#), [4](#)
- [6] Jacob Goldberger and Ehud Ben-Reuven. Training deep neural-networks using a noise adaptation layer. In *International conference on learning representations*, 2016. [2](#)
- [7] Bo Han, Quanming Yao, Xingrui Yu, Gang Niu, Miao Xu, Weihua Hu, Ivor Tsang, and Masashi Sugiyama. Co-teaching: Robust training of deep neural networks with extremely noisy labels. *Advances in neural information processing systems*, 31, 2018. [2](#), [6](#), [7](#)
- [8] Amine El Helou. Sensor har recognition app. matlab central file exchange. 2023. [1](#), [5](#)
- [9] Peter J Huber. Robust estimation of a location parameter. In *Breakthroughs in statistics: Methodology and distribution*, pages 492–518. Springer, 1992. [2](#)
- [10] Peter J. Huber. Robust Statistics. In *International Encyclopedia of Statistical Science*, pages 1248–1251. Springer Berlin Heidelberg, Berlin, Heidelberg, 2011. [1](#), [2](#)
- [11] Lu Jiang, Zhengyuan Zhou, Thomas Leung, Li-Jia Li, and Li Fei-Fei. Mentornet: Learning data-driven curriculum for very deep neural networks on corrupted labels. In *International conference on machine learning*, pages 2304–2313. PMLR, 2018. [2](#), [6](#)
- [12] Norman L Johnson, Samuel Kotz, and Narayanaswamy Balakrishnan. *Continuous univariate distributions, volume 2*. John wiley & sons, 1995. [5](#)
- [13] A Krizhevsky. Learning multiple layers of features from tiny images. Master’s thesis, University of Toronto, 2009. [7](#)
- [14] Yann LeCun. The mnist database of handwritten digits. <http://yann.lecun.com/exdb/mnist/>, 1998. [7](#)
- [15] Ricardo A Maronna, R Douglas Martin, Victor J Yohai, and Matías Salibián-Barrera. *Robust statistics: theory and methods (with R)*. John Wiley & Sons, 2019. [1](#)
- [16] Kevin P Murphy. *Probabilistic machine learning: Advanced topics*. MIT press, 2023. [2](#), [3](#), [4](#)
- [17] Duc Tam Nguyen, Chaithanya Kumar Mummadi, Thi Phuong Nhung Ngo, Thi Hoai Phuong Nguyen, Laura Beggel, and Thomas Brox. Self: Learning to filter noisy labels with self-ensembling. *arXiv preprint arXiv:1910.01842*, 2019. [6](#)
- [18] Muhammad Osama, Dave Zachariah, and Petre Stoica. Robust risk minimization for statistical learning from corrupted data. *IEEE Open Journal of Signal Processing*, 1:287–294, 2020. [2](#), [4](#), [5](#)
- [19] Giorgio Patrini, Alessandro Rozza, Aditya Krishna Menon, Richard Nock, and Lizhen Qu. Making deep neural networks robust to label noise: A loss correction approach. In *Proceedings of the IEEE conference on computer vision and pattern recognition*, pages 1944–1952, 2017. [2](#)
- [20] Hongxin Wei, Lei Feng, Xiangyu Chen, and Bo An. Combating noisy labels by agreement: A joint training method with co-regularization. In *Proceedings of the IEEE/CVF conference on computer vision and pattern recognition*, pages 13726–13735, 2020. [2](#), [6](#), [7](#)
- [21] Ross Wightman. Pytorch image models. <https://github.com/rwightman/pytorch-image-models>, 2019. [8](#)
- [22] Xiaobo Xia, Tongliang Liu, Bo Han, Chen Gong, Nannan Wang, Zongyuan Ge, and Yi Chang. Robust early-learning: Hindering the memorization of noisy labels. In *International conference on learning representations*, 2020. [2](#), [6](#), [7](#)
- [23] Yuanzhuo Xu, Xiaoguang Niu, Jie Yang, Steve Drew, Jiayu Zhou, and Ruizhi Chen. Usdnl: uncertainty-based single dropout in noisy label learning. In *Proceedings of the AAAI Conference on Artificial Intelligence*, pages 10648–10656, 2023. [2](#), [6](#), [7](#)
- [24] Zhilu Zhang and Mert Sabuncu. Generalized cross entropy loss for training deep neural networks with noisy labels. *Advances in neural information processing systems*, 31, 2018. [2](#)
- [25] Abdelhak M Zoubir, Visa Koivunen, Esa Ollila, and Michael Muma. *Robust statistics for signal processing*. Cambridge University Press, 2018. [4](#)

Adaptive Parameter-Free Robust Learning using Latent Bernoulli Variables

Supplementary Material

Optimization w.r.t. probabilities π is convex

Using $\langle \cdot \rangle$ to denote the mean of vector entries, we express the Hessian of $\mathcal{L}(\theta, \pi)$ w.r.t. π ,

$$\nabla_{\pi}^2 \mathcal{L} = \text{diag} \left(\frac{1}{\pi(1-\pi)} \right) - \frac{\mathbf{1} \cdot \mathbf{1}^{\top}}{n \langle \pi \rangle \langle 1 - \pi \rangle}. \quad (21)$$

Convexity in π requires $\nabla_{\pi}^2 \mathcal{L}$ to be positive semi-definite, i.e., for any $\mathbf{x} \neq 0$,

$$\mathbf{x}^{\top} \nabla_{\pi}^2 \mathcal{L} \mathbf{x} = \sum_{i=1}^n x_i^2 \cdot \frac{n \langle \pi \rangle \langle 1 - \pi \rangle - \pi_i (1 - \pi_i)}{\pi_i (1 - \pi_i) n \langle \pi \rangle \langle 1 - \pi \rangle} \geq 0. \quad (22)$$

Given that $\pi \in [0; 1]^n$, the denominator cannot be negative, and therefore we only require to verify the sign of

$$\sum_{i=1}^n \left[n \langle \pi \rangle \langle 1 - \pi \rangle - \pi_i (1 - \pi_i) \right] \quad (23)$$

$$= \sum_{i=1}^n \pi_i \sum_{j=1}^n (1 - \pi_j) - \sum_{i=1}^n \pi_i + \sum_{i=1}^n \pi_i^2 \quad (24)$$

$$= (n-1) \sum_{i=1}^n \pi_i - \sum_{i,j=1}^n \pi_i \pi_j + \sum_{i=1}^n \pi_i^2 \quad (25)$$

$$= \sum_{i=1}^n \pi_i \left[n-1 - \sum_{\substack{j=1 \\ j \neq i}}^n \pi_j \right] \stackrel{?}{\geq} 0. \quad (26)$$

Here, ‘?’ sign implies that we need to check if the final expression is not negative to prove positive semi-definiteness. However, in the last expression, $\pi_i \geq 0$ and $n-1 \geq \sum_{\substack{j=1 \\ j \neq i}}^n \pi_j$ for any $i = 1, \dots, n$. Therefore, $\nabla_{\pi}^2 \mathcal{L}$ is positive semi-definite, and minimization of $\mathcal{L}(\theta, \pi)$ w.r.t. π is a convex optimization problem.

Convexity of $\mathcal{L}(\theta, \pi)$ in π allows for efficient computation of Bernoulli probabilities π_i , $i = 1, \dots, n$. In our implementation, we use the fixed-point algorithm to find the solution for the corresponding first-order necessary conditions $\nabla_{\pi} \mathcal{L} = 0$. Another option would be, for example, to use the Newton’s method, which requires inverting the Hessian $\nabla_{\pi}^2 \mathcal{L}$. But this matrix has rank one, and therefore can be inverted efficiently in $O(n)$ operations using the Woodbury formula. Also note that, when using the fixed-point algorithm (17), one needs to compute the exponential of the loss value for each sample. To avoid numerical issues and ensure convergence, we scale the range of the loss values with a constant (we divide by the average loss).

Online learning with varying level of noise

In Figure 7, we provide the performance metrics of the standard SGD approach, RRM, and RLVI, used for binary classification of data that arrives in batches with varying number of outliers. In this figure, we show both accuracy and recall values for all three methods.

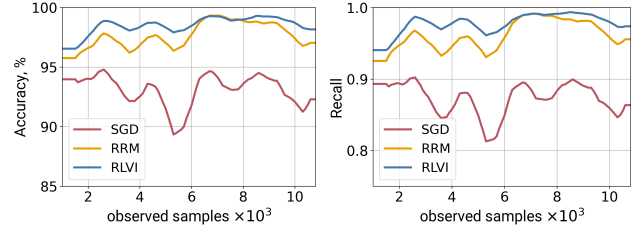


Figure 7. Online classification. Accuracy (left) and recall (right) on left-out data versus total number of observed samples – the metric is smoothed with a moving average filter.

Image classification with synthetic noise

Figures 8 to 13 are the plots, similar to Figure 5, showing the results of image classification after training on the data corrupted with three types of synthetic noise at corruption level ε equal to 0.2 and 0.45. We also provide the ratio of correctly identified corrupted and non-corrupted images based on the introduced criterion. These figures show that, although type II error is not always below 5%, overfitting is reduced in all settings, and RLVI achieves a higher accuracy than the standard method in all problem instances.

Image classification with real noise

In case of the Food101 dataset, a part of the training images is mislabeled. The ratio of such images, ε , is unknown, and thus we run the robust learning algorithms that depend on this hyperparameter: Co-teaching, JoCoR, CDR, and USDNL, using different estimates of ε (40%, 20%, 10%, 5%, 3%, and 1%). Figure 14 presents the accuracy of different methods on the manually cleaned testing set from Food101. As the estimate of ε used in training decreases, the accuracy of alternative methods improves and becomes optimal with ε around 3%. In this experiment, RLVI achieved the best results when no regularization was used. This can be attributed to the weaker overfitting in the case of the Food101 dataset, as compared to examples with synthetic noise: test accuracy for RLVI without regularization in Figure 14 gradually increases, in contrast to the corresponding curve in Figure 5.

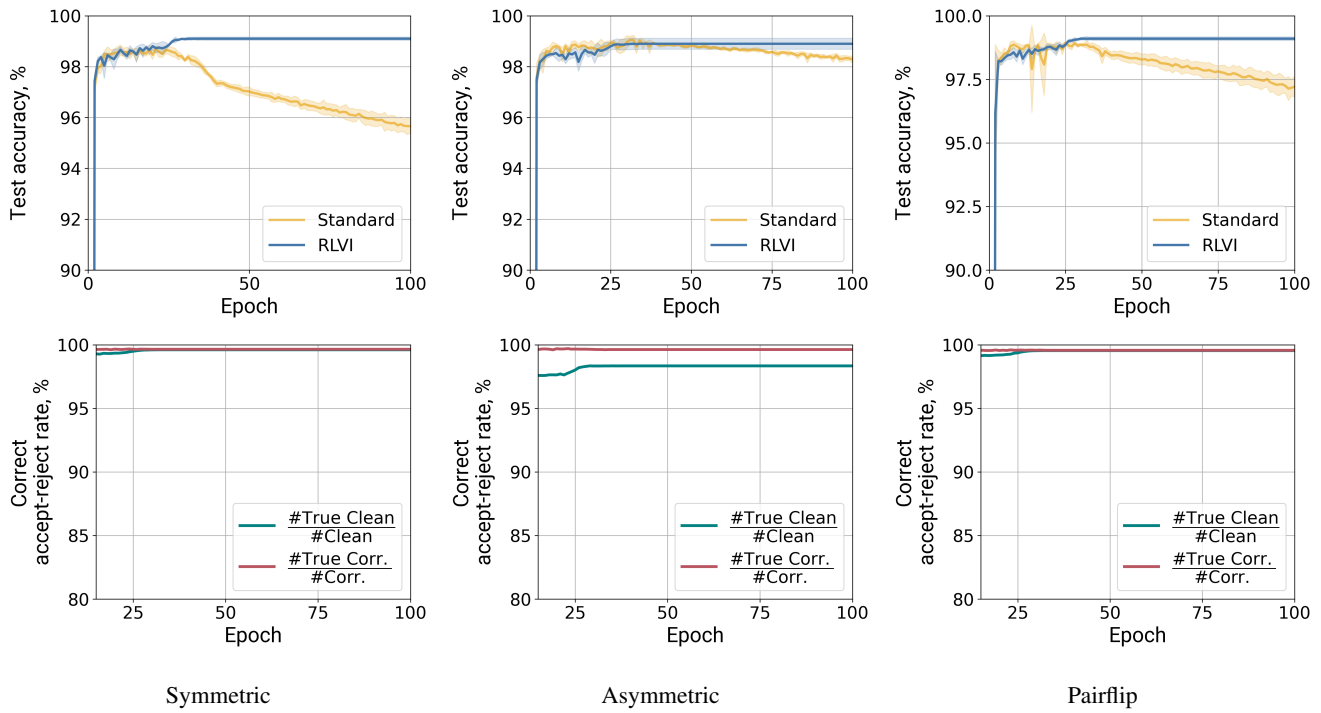


Figure 8. MNIST, 20% noise rate. *Top*: test accuracy (mean \pm st. dev. over 5 runs). *Bottom*: type I and type II errors (mean over 5 runs).

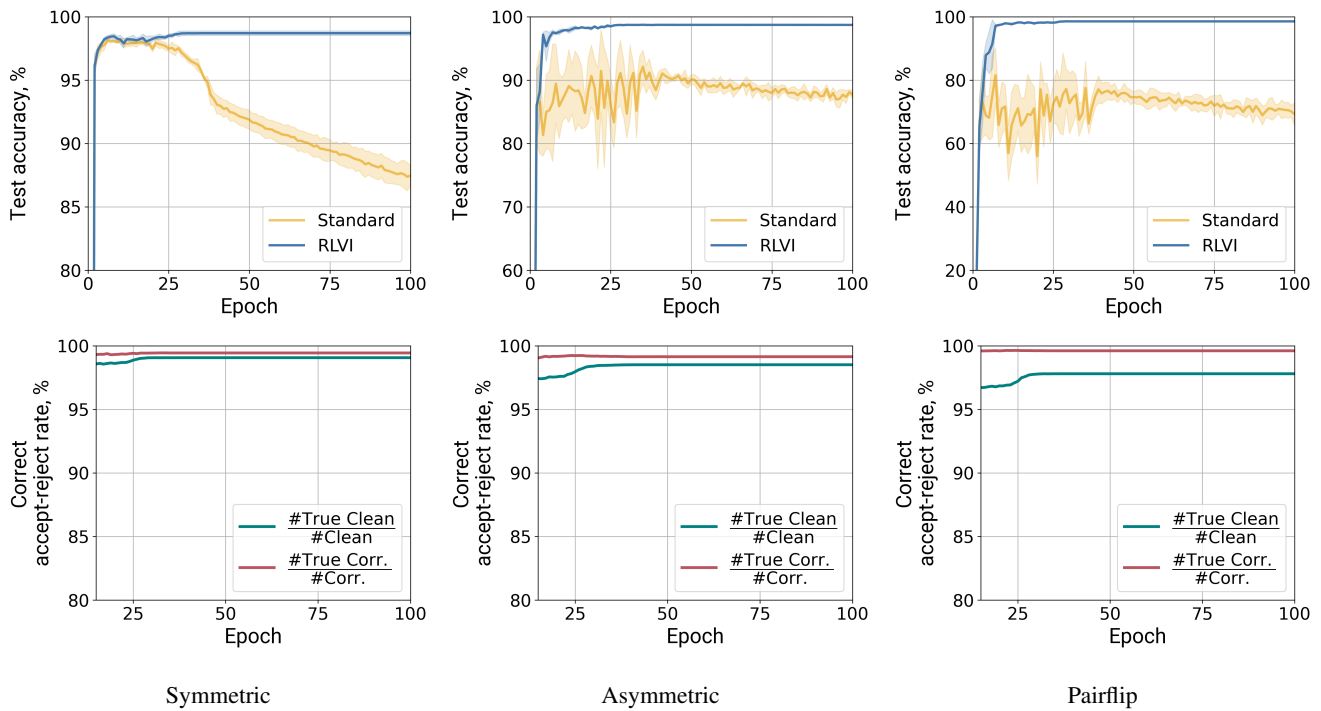


Figure 9. MNIST, 45% noise rate. *Top*: test accuracy (mean \pm st. dev. over 5 runs). *Bottom*: type I and type II errors (mean over 5 runs).

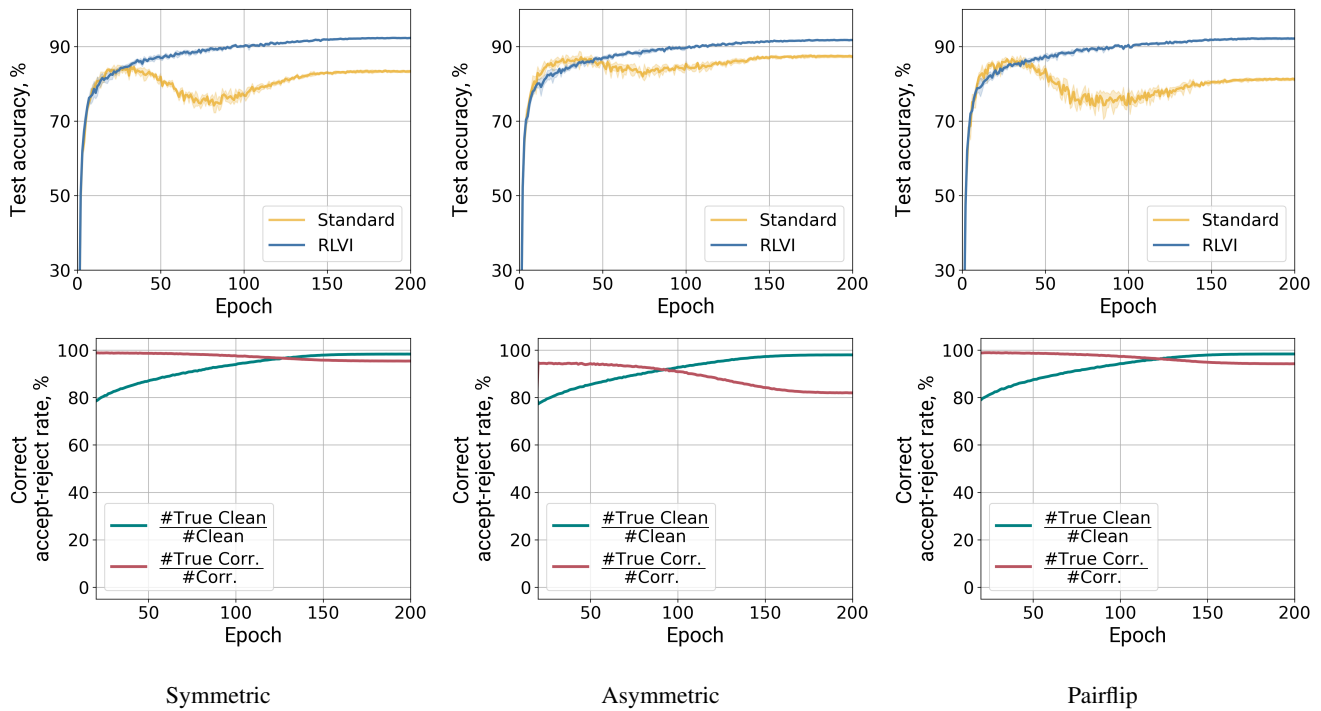


Figure 10. CIFAR10, 20% noise rate. *Top*: test accuracy (mean \pm st. dev. over 5 runs). *Bottom*: type I and type II errors (mean over 5 runs).

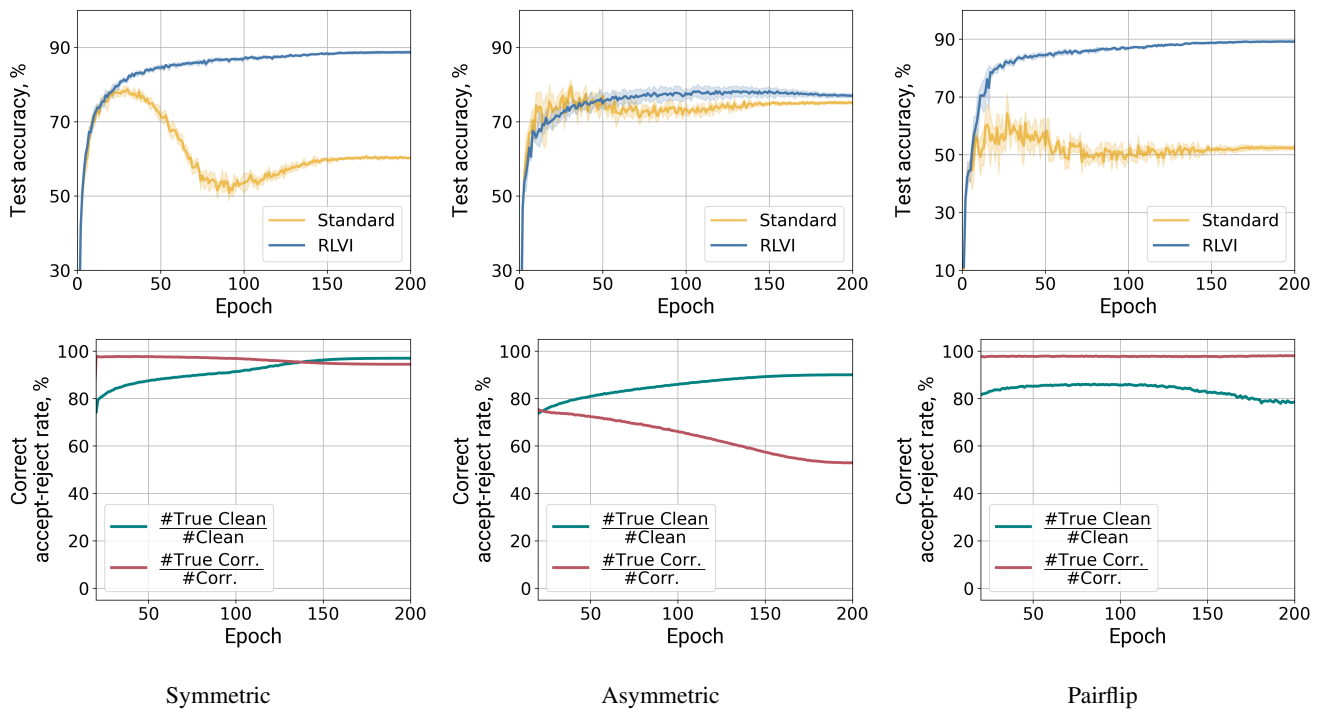


Figure 11. CIFAR10, 45% noise rate. *Top*: test accuracy (mean \pm st. dev. over 5 runs). *Bottom*: type I and type II errors (mean over 5 runs).

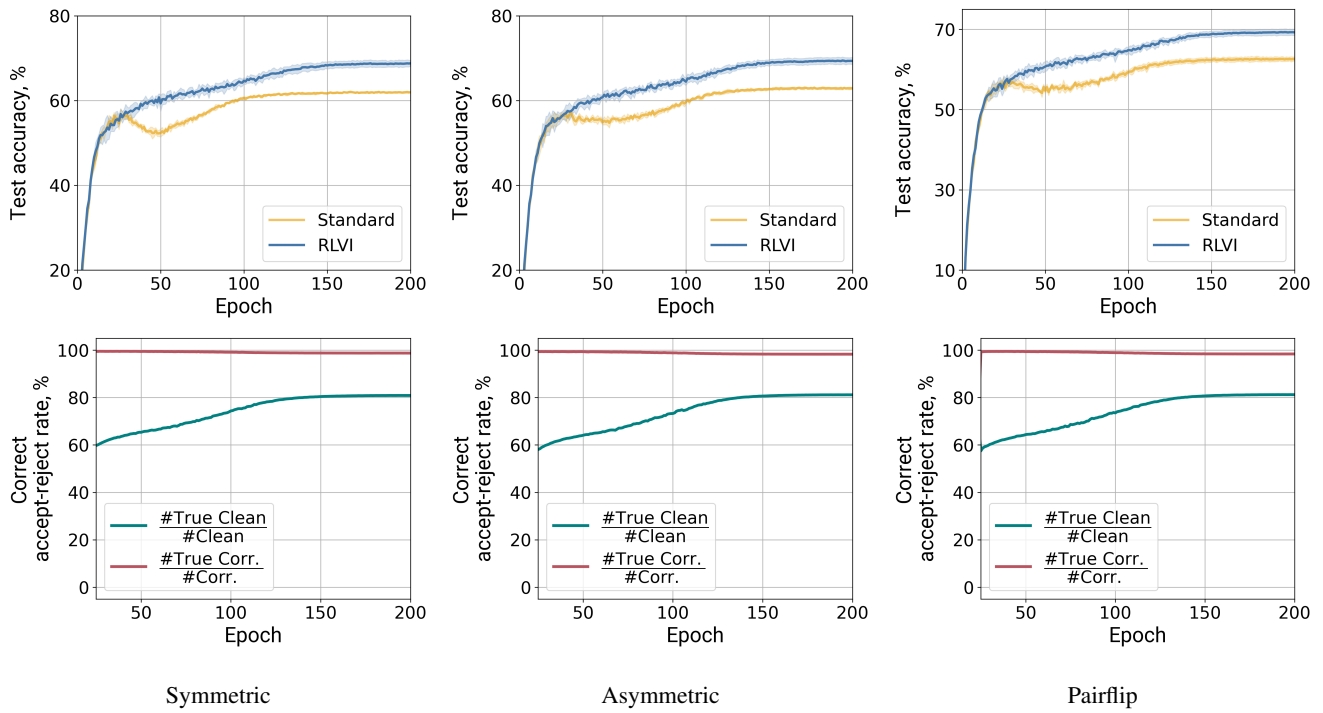


Figure 12. CIFAR100, 20% noise rate. *Top*: test accuracy (mean \pm st. dev. over 5 runs). *Bottom*: type I and type II errors (mean over 5 runs).

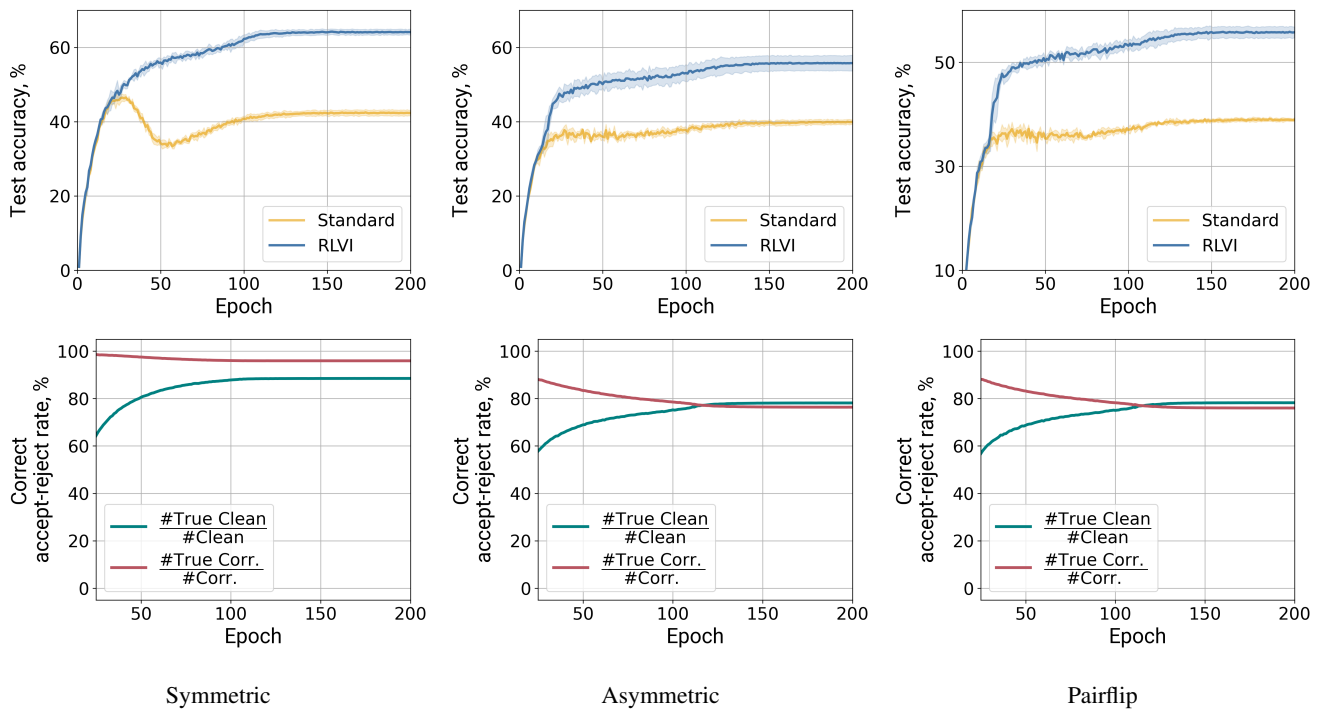


Figure 13. CIFAR100, 45% noise rate. *Top*: test accuracy (mean \pm st. dev. over 5 runs). *Bottom*: type I and type II errors (mean over 5 runs).

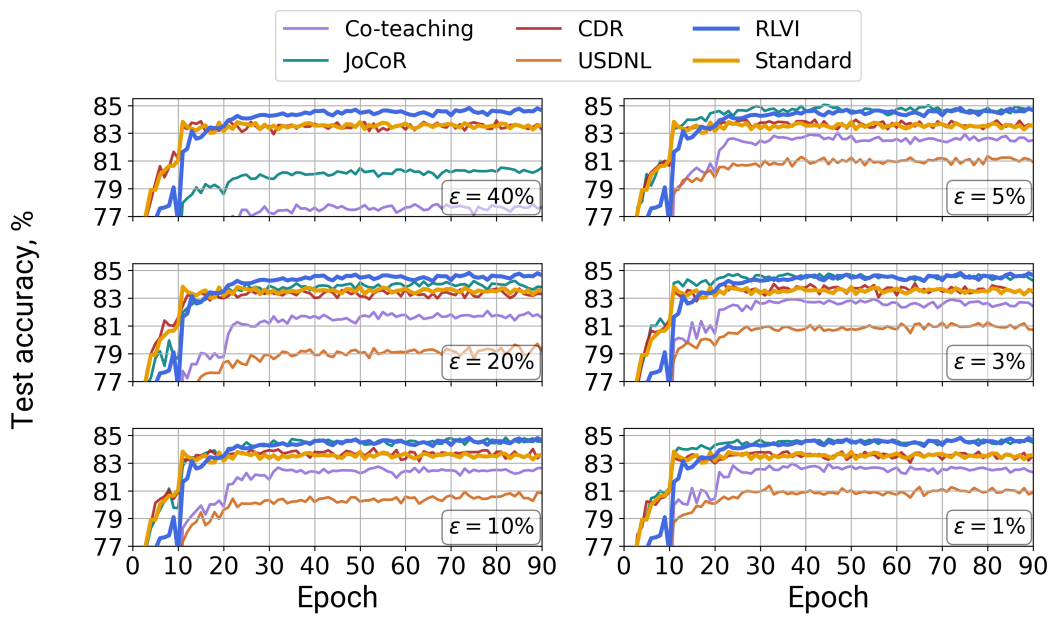


Figure 14. Test accuracy (%) for Food101, using different estimates of corruption level ϵ for Co-teaching, JoCoR, CDR, and USDNL.